SUPPLEMENTARY MATERIALS

The present file contains the supplementary materials associated with the “Tumor-associated macrophage clusters linked to immunotherapy in a pan-cancer census” publication. In particular, it contains the following sections:

1. Supplementary Figures

2. Supplementary Tables

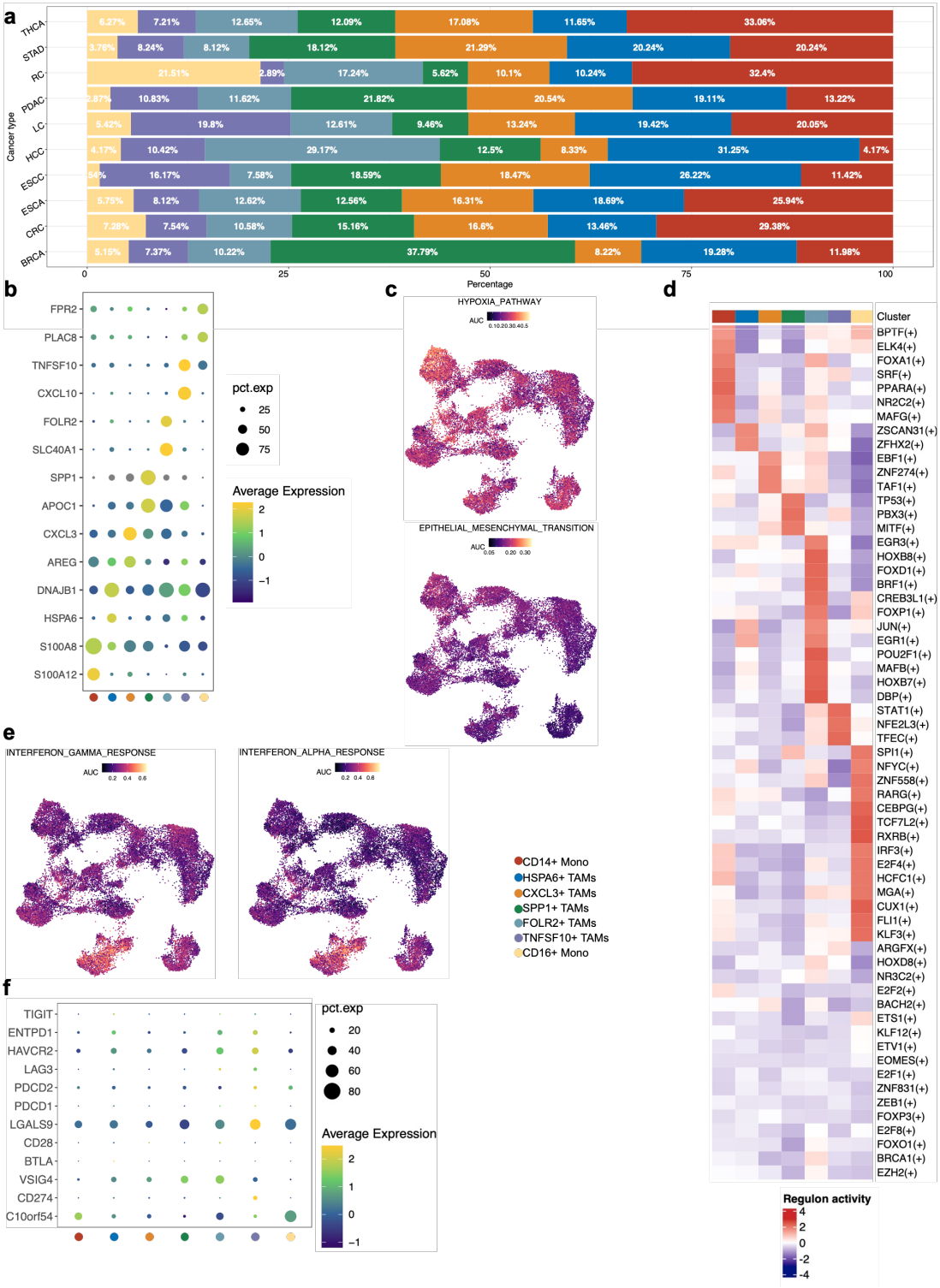

Supplementary Figure 1 Proportions, marker expression, gene signatures, and regulon analysis of monocyte/TAM clusters across nine cancer types. a Stacked bar plots illustrate the proportion of all monocyte/TAM clusters across nine cancer types. **b** The expression of selected markers of seven monocyte/TAM clusters. **c** UMAPs of Monos/TAMs clusters colored by expression of AUCell for gene signatures derived for Hypoxia and EMT from MSigDB. **d** Heatmap showing relative expression levels of differentially expressed regulons in Monos/TAMs clusters as revealed by a SCENIC analysis. **e** UMAPs of Monos/TAMs clusters

colored by expression of AUCell for gene signatures derived for IFN-γ/α response from MSigDB. **f** The expression of co-inhibitory/co-stimulatory molecules of seven monocyte/TAM clusters.

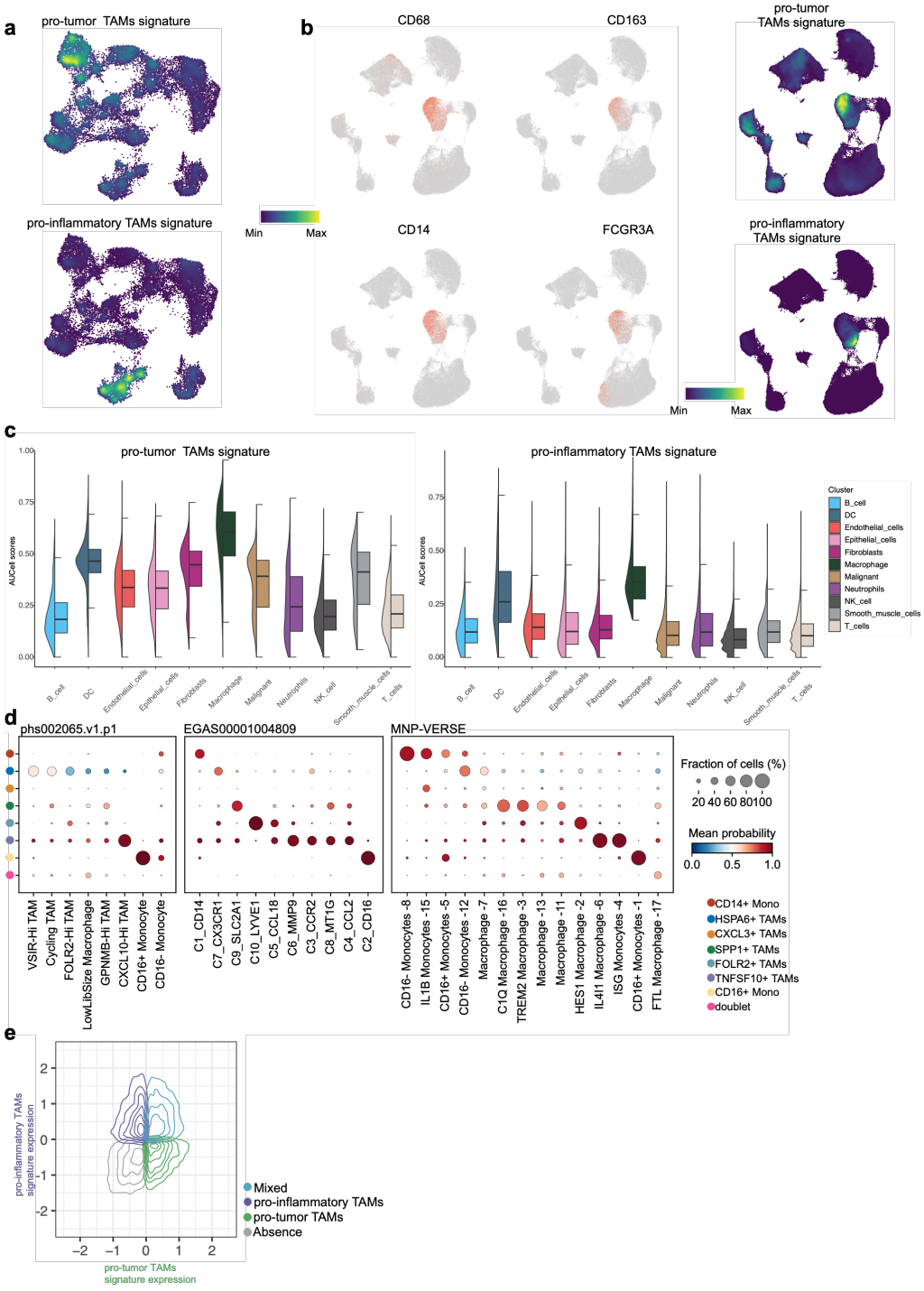

Supplementary Figure 2 Marker expression, gene signatures, and cell type comparison of Mono/TAM clusters in pan-cancer datasets. a UMAP analysis revealed seven Mono/TAM clusters, each colored according to the AUCell score for pro-inflammatory and pro-tumor TAM signatures within our pan-cancer dataset. This analysis specifically retained genes unique to the TNFSF10+ and SPP1+ TAM clusters. **b** left: UMAP visualization of clusters colored by the

monocyte/macrophage markers (CD14, FCGR3A, CD68, and CD163) representing major cell types in the GSE183904 dataset; right: UMAP for major cell type clusters colored by the AUCell score of the pro-inflam and pro-tumor TAMs signatures in the GSE183904 dataset. **c** Violin plots depicting AUCell scores for gene signatures derived for pro-inflam and pro-tumor TAMs across all major cell type clusters in the pan-cancer scRNA-seq from Barkley et al. **d** Cell types and annotations of our study (rows) were compared with annotations (columns) reported by three previous scRNA-seq studies using CellTypist. The size of the dots represents the proportion of cells predicted to be certain cell types, and the color scale represents the average probability of prediction. **e** The contour density plot illustrates the differential expression profiles of co-expressed pro-inflammatory and protumor TAMs signatures distribution across 32 different cancer types.

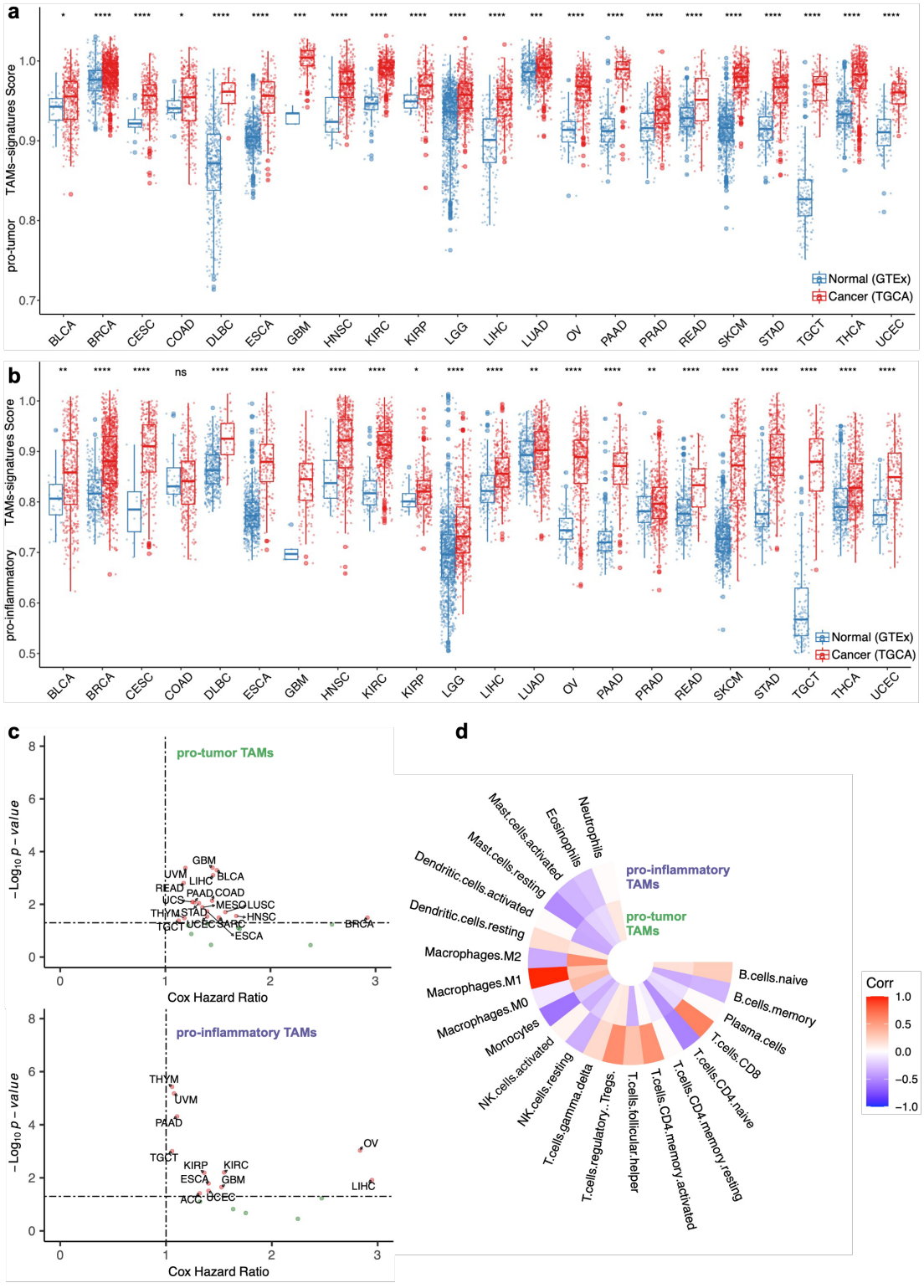

Supplementary Figure 3 Distribution of TAMs signature scores, survival prediction, and correlation with immune-infiltrating cells across TCGA tumor and normal samples. a Distribution of pro-tumor TAMs signature score calculated by ssGSEA across indicated tumor samples (TCGA, n = 8,171) compared with normal samples from GTEx (n = 5,680). **b** Distribution of pro-inflam TAMs signature score calculated by ssGSEA across indicated tumor samples (TCGA, n = 8,171) compared with normal samples from GTEx (n = 5,680). **c** Overall

survival prediction with Cox proportional hazard ratio and −log10(P value) based on two-sided log-rank testing across the pan-TCGA dataset using pro-tumor and pro-inflam TAMs signature score. **d** Correlation plots of pro-tumor and pro-inflam TAMs signature score and the immune-infiltrating cells determined based on the CIBERSORT algorithm and the IPS.

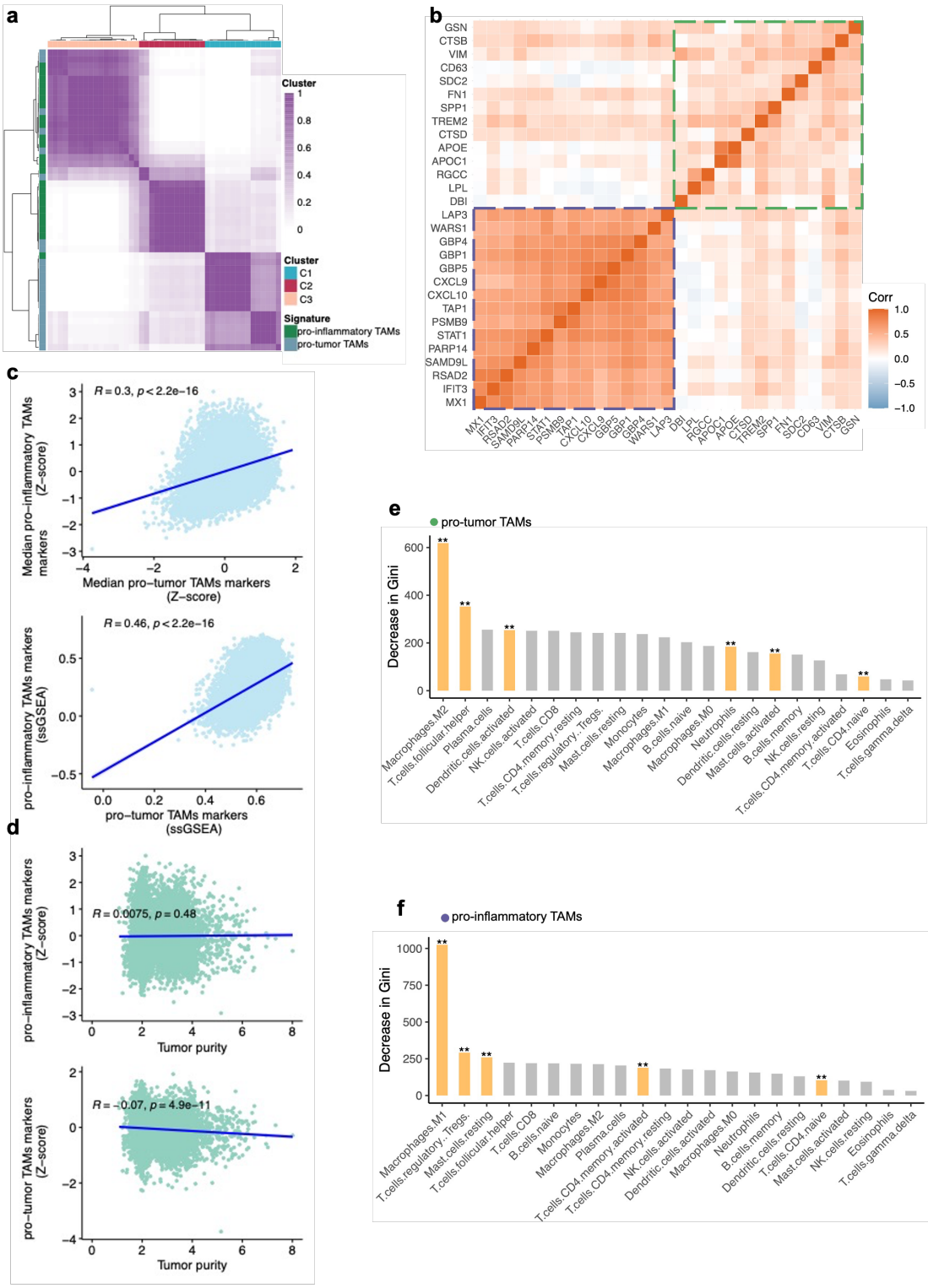

Supplementary Figure 4 Principal component analysis, gene correlation matrix, and predictive importance of immune cells for pro-inflammatory and pro-tumor TAMs. a Principal component analysis showed that the expression of the pro-inflam TAMs and pro-

tumor TAMs signature represents distinct TAMs phenotypes. **b** Gene-by-gene correlation matrix visualizing the pairwise Spearman correlation coefficients in the pan-TCGA dataset. **c** Correlation curves between pro-inflammatory and pro-tumor TAMs based on z scores and ssGSEA in the pan-TCGA dataset. Each dot represents one tumor. P values from Pearson correlation test. **d** Correlation curves between pro-inflammatory and pro-tumor TAMs based on z scores and tumor purity in the pan-TCGA dataset. Each dot represents one tumor. P values from Pearson correlation test. **e-f** Random-forest predictor importance (the value of decrease Gini score) of 22 immune cells as drivers for pro-inflammatory and pro-tumor TAMs. The accuracy importance measure was computed for each tree and averaged over the forest (500 trees). Higher decrease Gini score imply more important predictors. Significance levels are as follows: **P < 0.01.

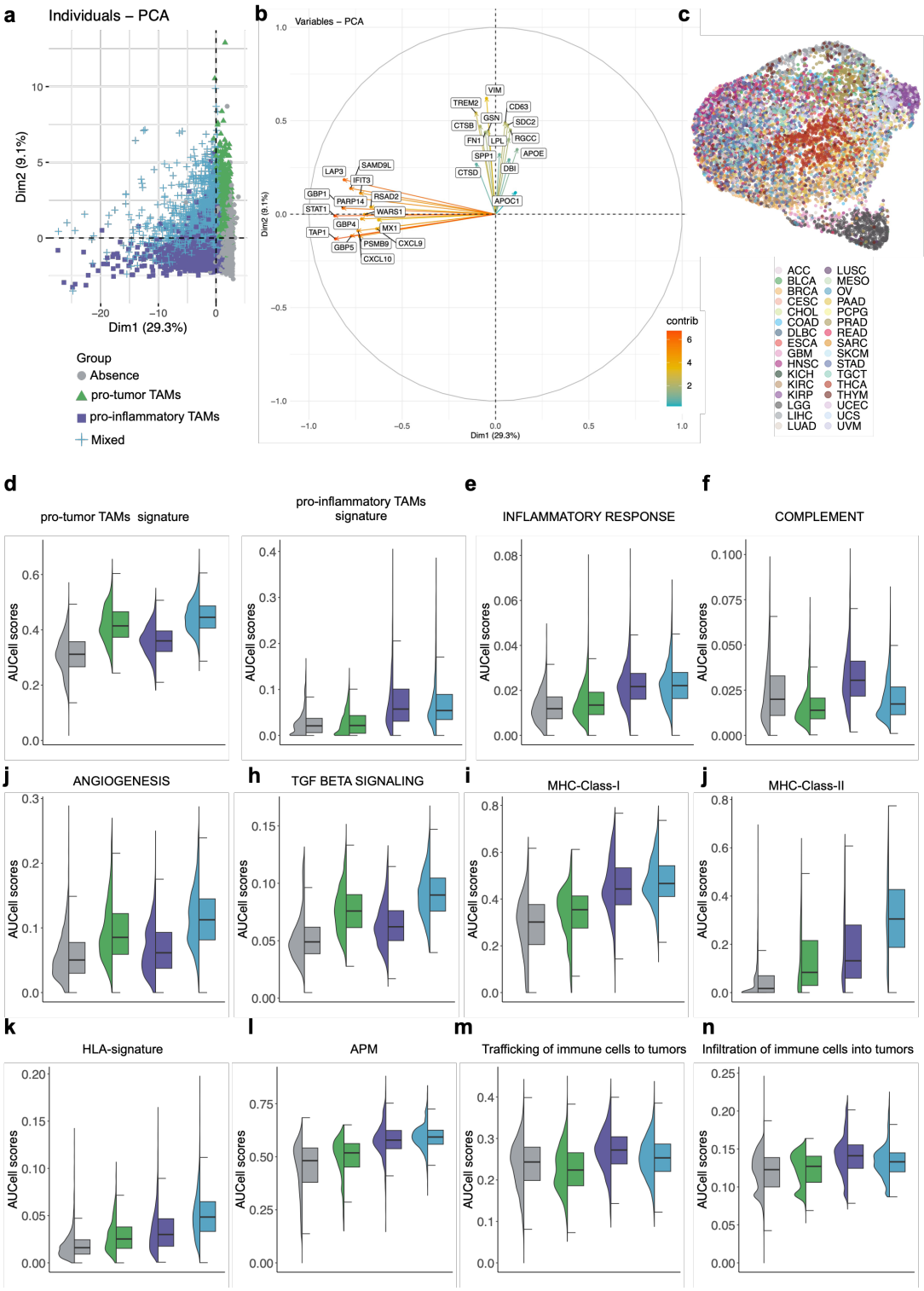

Supplementary Figure 5 PCA analyze, AUCell scores for TAMs and immune-related gene signatures across TCGA's Pan-Cancer Atlas. a PCA analysis on the abundance of pro-inflam and pro-tumor TAMs components in the TCGA's Pan-Cancer Atlas using the co-expressed pro-inflam and pro-tumor TAMs genes. **b** The co-expressed pro-inflam and pro-tumor TAMs genes are plotted as PCA analysis variables. Positive correlated variables point to the same side of the plot. Negative correlated variables point to opposite sides of the graph. **c** UMAP display color-coded by 33 cancer types using Louvain clustering to cluster patients in the TCGA's Pan-Cancer

Atlas. Each dot represents a single patient. **d** Violin plots depicting AUCell scores for gene signatures derived for pro-inflam and pro-tumor TAMs across four subgroups of the TCGA's Pan-Cancer Atlas. **e-h** Violin plots depicting AUCell scores for gene signatures derived for the partial MSigDB Hallmark gene sets across four subgroups of the TCGA's Pan-Cancer Atlas. **i-n** Violin plots depicting AUCell scores for gene signatures derived for the immune-related pathways across four subgroups of the TCGA's Pan-Cancer Atlas.

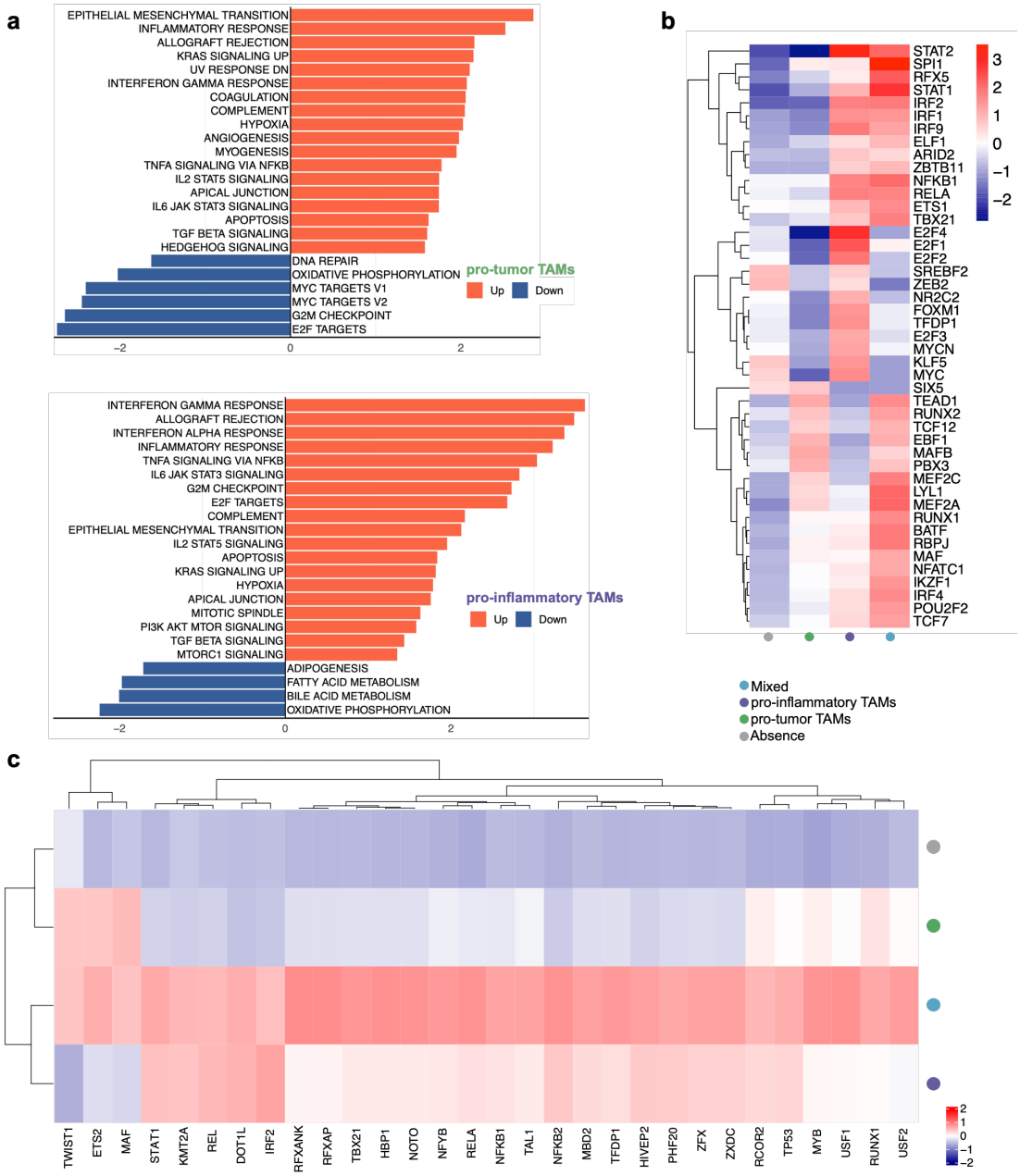

Supplementary Figure 6 Hallmark gene sets and transcription factor analysis of pro-inflammatory and pro-tumor TAMs subtypes in TCGA's Pan-Cancer Atlas. a MSigDB Hallmark gene sets associated with pro-inflam TAMs and pro-tumor TAMs subtype, respectively. **b** Transcription factor analysis of four subtypes stratified by pro-inflam TAMs and pro-tumor TAMs in the TCGA's Pan-Cancer Atlas using DoRothEA. **c** Transcription factor analysis of four subtypes stratified by pro-inflam TAMs and pro-tumor TAMs in the TCGA's Pan-Cancer Atlas using decoupleR.

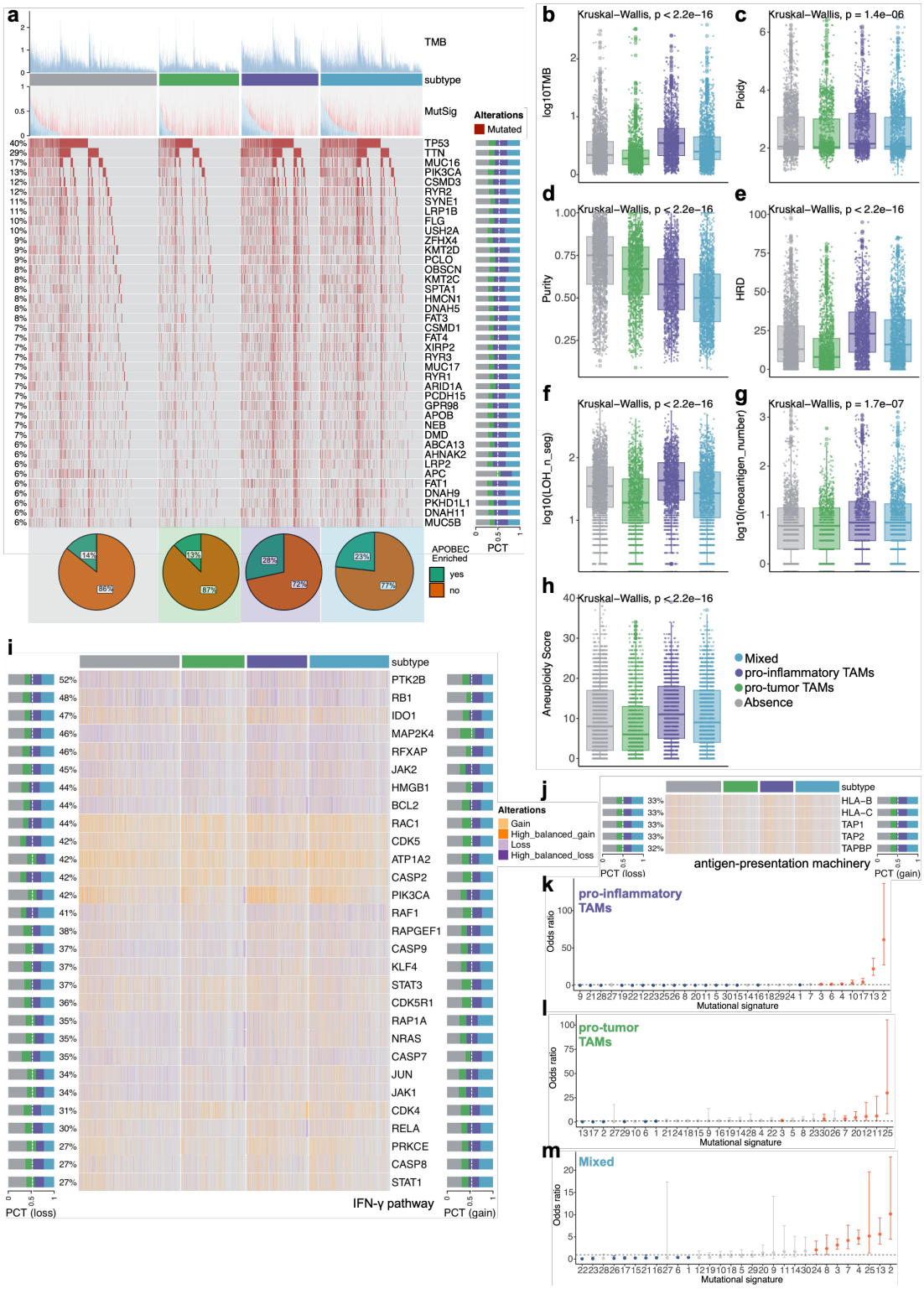

Supplementary Figure 7 Genomic alterations, mutational signatures, and tumor characteristics stratified by pro-inflammatory and pro-tumor TAMs in TCGA's Pan-Cancer Atlas. a Oncoprint of genomic alterations in at least 6% of the TCGA's Pan-Cancer Atlas stratified by pro-inflam TAMs and pro-tumor TAMs. Samples are ordered after the combined contribution of the APOBEC-related mutational signatures. Panels: TMB, relative contribution of APOBEC-related mutational signatures, mutated genes, pie charts showing the APOBEC-enriched and non-APOBEC enriched samples. **b-h** TMB, tumor ploidy/purity, HRD,

LOH, neoantigen load, and aneuploidy score according to the four subtypes stratified by pro-inflam TAMs and pro-tumor TAMs in the TCGA's Pan-Cancer Atlas. **i** copy number alterations of selected IFN-γ pathway driver genes. **j** copy number alterations of selected antigen-presentation machinery pathway driver genes. **k-m** Associations between mutational signatures and pro-inflam TAMs, pro-tumor TAMs, and mixed subtypes. Statistically significant associations obtained from multinomial logistic regression are shown in red. The central measure is the parameter estimate, and the error bars indicate 95% CI; the horizontal dashed line corresponds to an OR of 1.

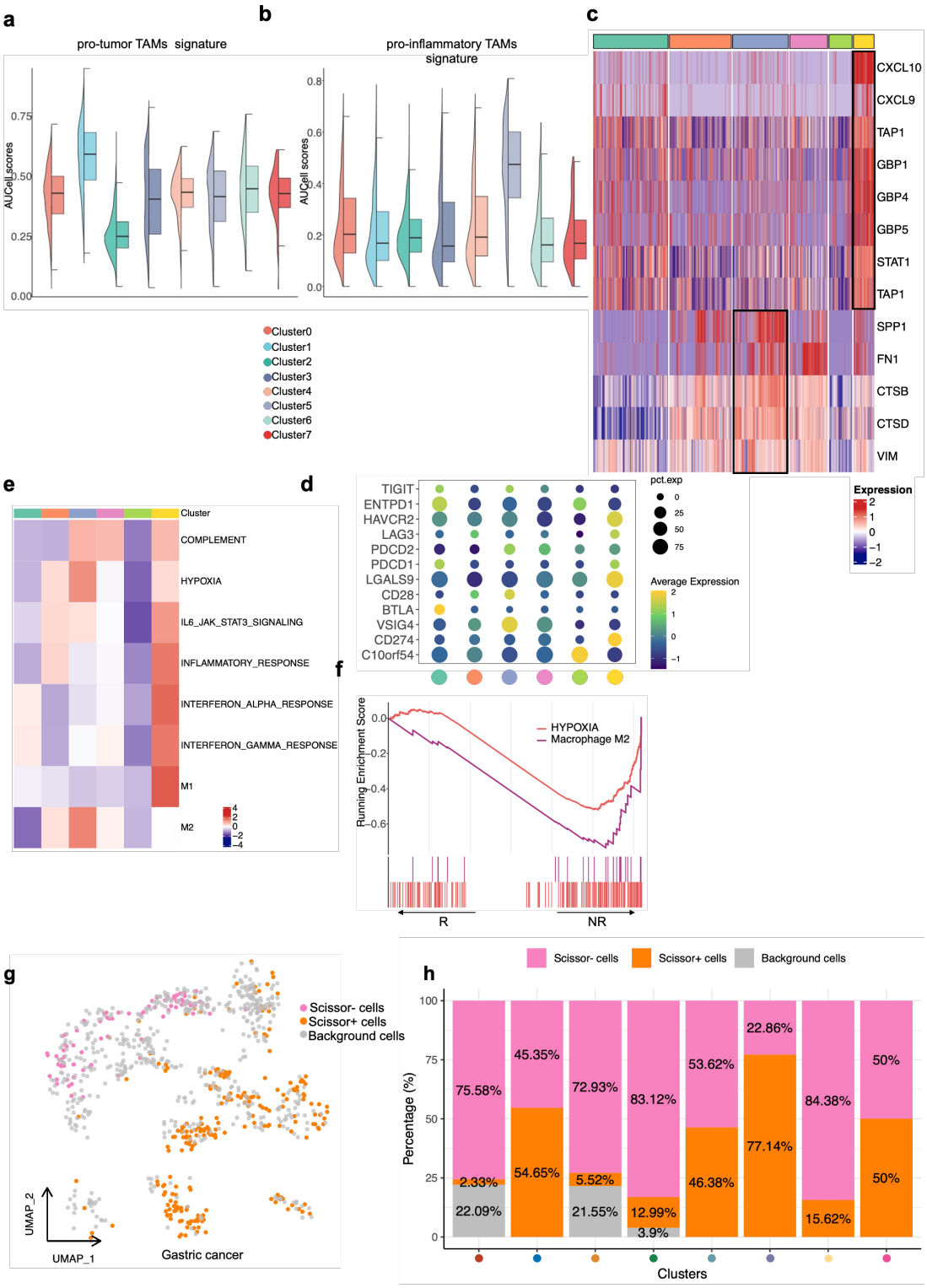

Supplementary Figure 8 Analysis of pro-inflammatory and pro-tumor TAMs markers, pathway activities, and ICB responses. a-b Violin plots depicting AUCell scores for gene signatures derived for pro-inflam and pro-tumor TAMs across all re-clustered monocytes/macrophages in the phs002065 dataset. **c** Heatmaps for monocytes/macrophages clusters in the GSE120575 dataset for select pro-inflam and pro-tumor TAMs markers highlighted. **d** The expression of co-inhibitory/co-stimulatory molecules of monocytes/macrophages clusters in the GSE120575 dataset. **e** Heatmap shows difference in

pathway activities scored by GSVA per cell between different monocytes/macrophages clusters in the GSE120575 dataset. **f** GSEA shows enriched pathways in the Cluster5 (ICB responders) in the GSE120575 dataset. R: responders including ICB CR/PR patients; NR: non-responders including ICB SD/PD patients. **g** UMAP visualization of the Scissor-selected cells in our integrated scRNA-seq dataset containing only GC cells. The orange and pink dots are Scissor+ (ICB responses) and Scissor- (ICB non-responses) cells, respectively. **h** Stacked bar plots illustrate the proportion of all Scissor+ and Scissor− cells across eight monocyte/TAM clusters in our integrated scRNA-seq dataset containing only GC cells.

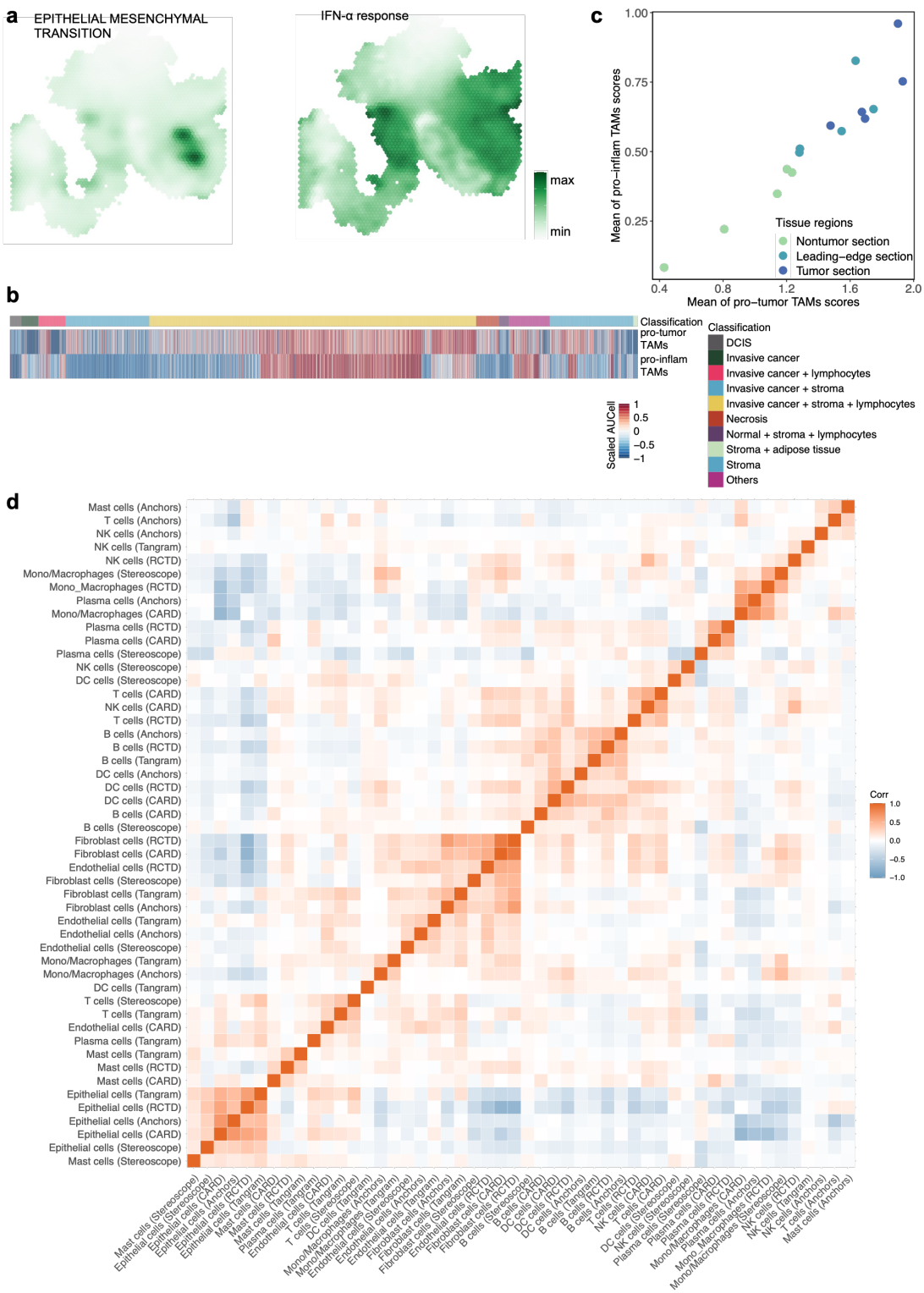

Supplementary Figure 9 IFN-α and epithelial-mesenchymal transition, TAMs signatures, and integration methods correlation. a Surface plot of IFN-α, and epithelial mesenchymal transition in the S1 tumor sample. **b** Scores of the pro-inflam and pro-tumor TAMs signatures across the six cases using the AUCell method. Values signify the scaled AUCell score per spots (columns) and are grouped by pathology annotation. **c** Scatterplot of the mean pro-inflam TAMs score versus the mean and pro-tumor TAMs score. Each dot indicated one spatial transcriptomics cluster from Chen et al. **d** Correlation matrix for all five integration methods

and all ten major cell types.

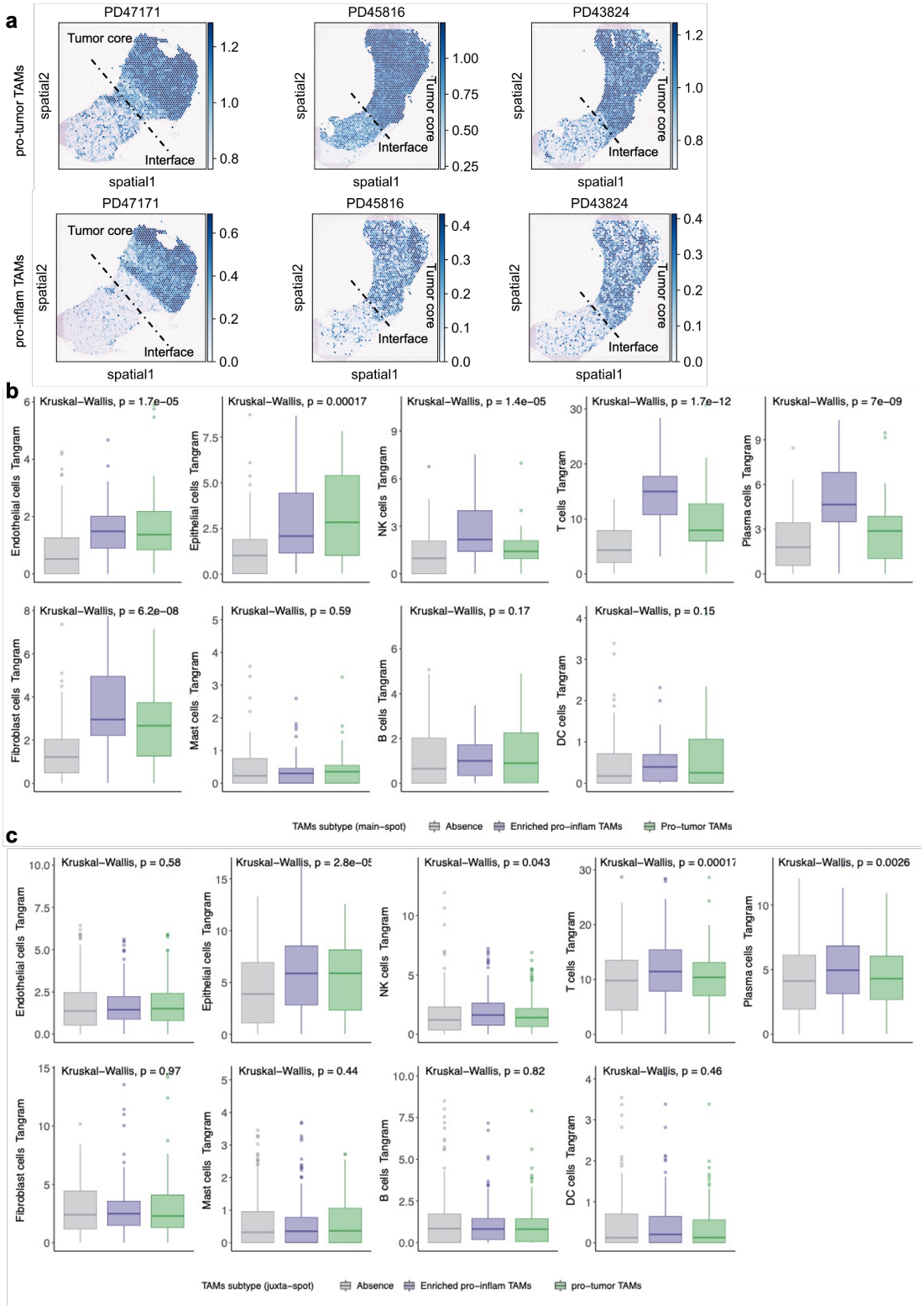

Supplementary Figure 10 Spatial mapping of TAMs and cell type fractions in different TAMs subtypes. a Spatial mapping of two TAMs is performed on representative tumor-normal interface samples (PD47171, PD45816, and PD43824) from the study by Thomas et al., utilizing signature scores. The estimated abundance, represented by color intensity, is superimposed on a histological image. **b** Boxplots of the fractions of nine major cell types in

main spots of mono/macrophages across four samples identified by Tangram. **c** Boxplots of the fractions of nine major cell types in juxta spots of mono/macrophages across four samples identified by Tangram.

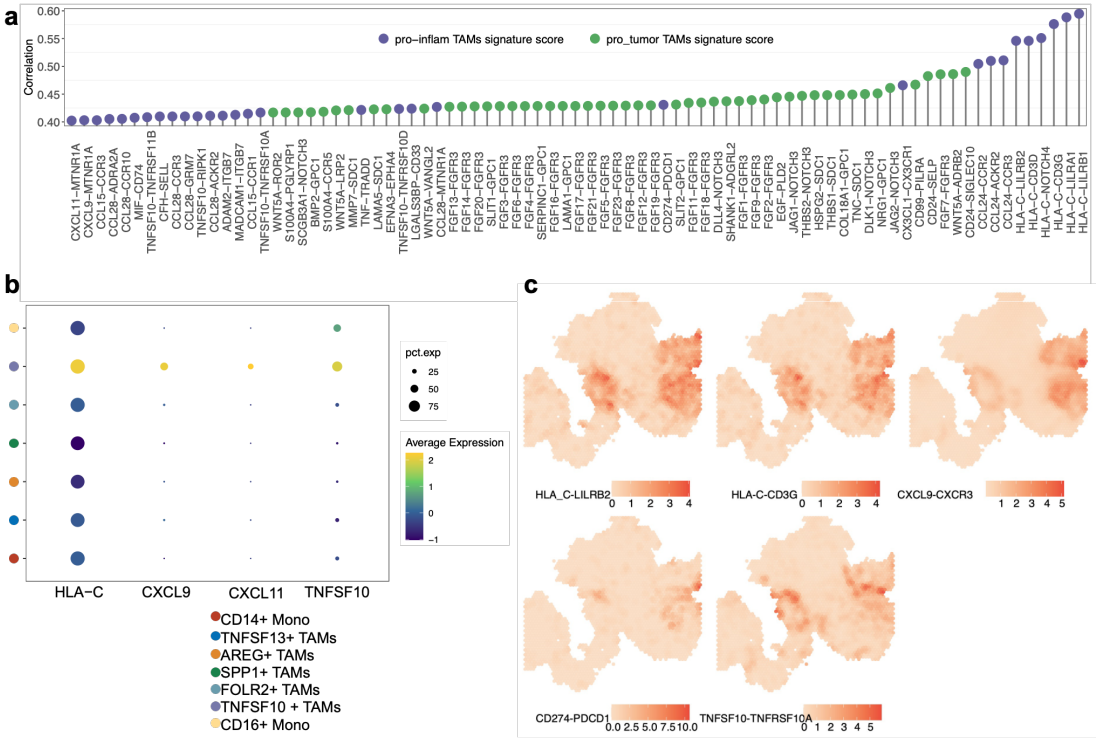

Supplementary Figure 11 Correlation analysis and expression of ligand-receptor pairs. a The correlation between the interaction expression of ligand-receptor pairs and pro-inflam and pro-tumor TAMs signatures through Spearman correlation analysis. The length of the vertical line indicates the correlation. **b** The expression of selected markers of seven monocyte/TAM clusters. **c** Surface plot of the ligand-receptor pairs in the S1 tumor sample.

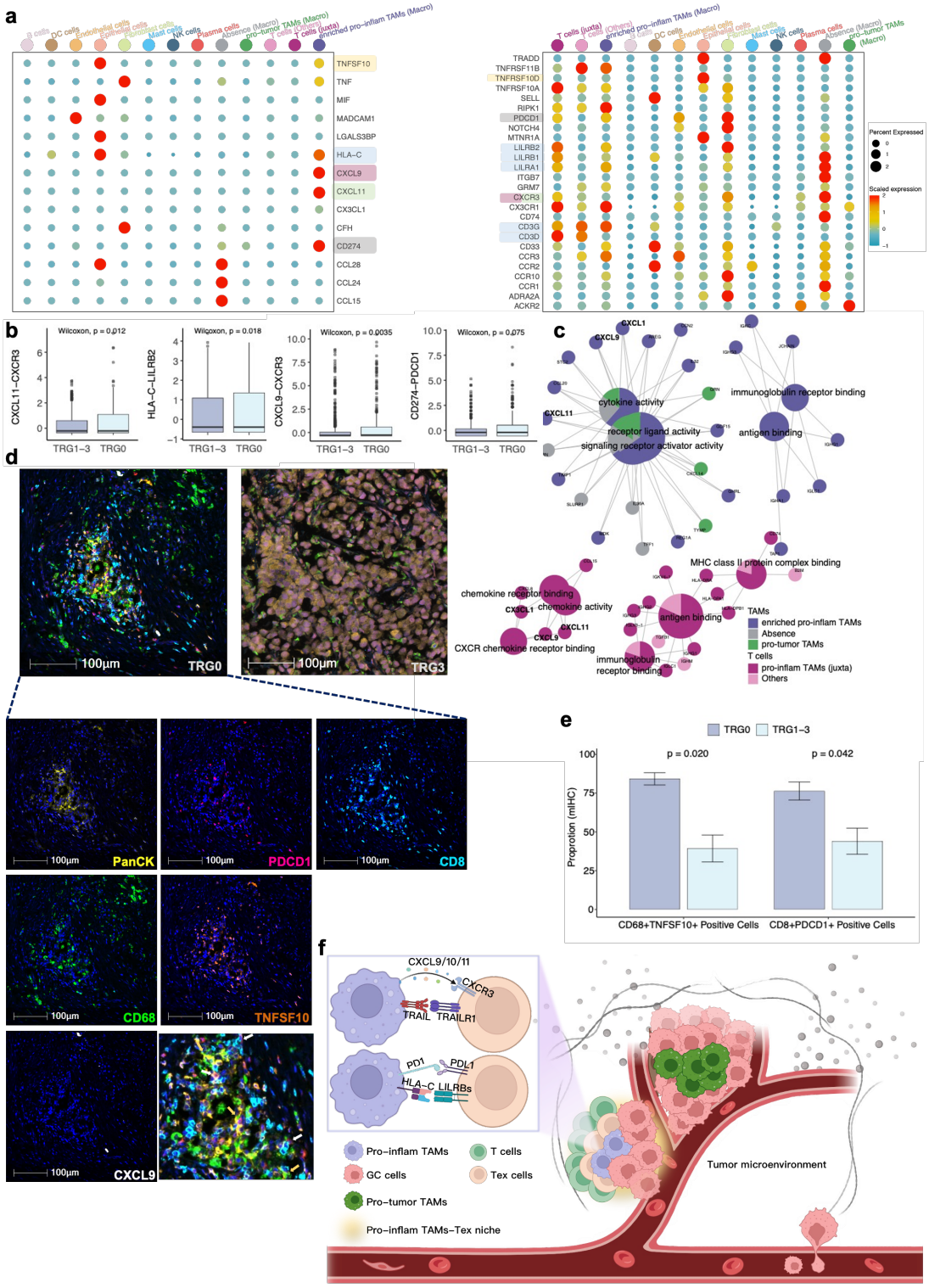

Supplementary Figure 12 Ligand-receptor interactions, GO enrichment analysis, and spatial distribution model of TAMs in the TME. a Dot plots showing expression of CellTalkDB relevant ligands in epithelial, stromal and fibroblast with cognate receptors. Only significant interactions ($r > 0.4$ and FDR < 0.05) are represented. The color of the boxes corresponds to the pathways whose ligand–receptor partners are involved. **b** Boxplots of the ligand-receptor pairs interaction expression in the TRG0 and TRG1-3. Each datapoint represents the expression level of matched ligand-receptor pairs within pro-inflam TAM spots

and their neighborhood, as determined by spatial co-expression analysis. The P value was based on a Wilcoxon signed-rank test. **c** GO enrichment analysis of top enriched pathways in the pro-inflam TAMs-Tex niches. **d** Staining of TAMs (CD68) and CD8+T cells. Representative cells are indicated by arrows, including TNFSF10+ CD68 + cells (yellow) and PD-1 + CD8+ cells (white). Scale bars, 100 μm. **e** Cellular proportional changes of CD68+TNFSF10+TAMs and CD8+ PDCD1 T cells in the TRG0 and TRG1-3 samples revealed by mIHC; 12 patients were classified as having TRG 1-3, while four were categorized as TRG0; P values were determined by the Wilcoxon test. **f** Schematic illustration of our proposed model for spatial distribution of pro-inflam and pro-tumor TAMs in the TME. Figures created using BioRender (biorender.com) with authorised permission.

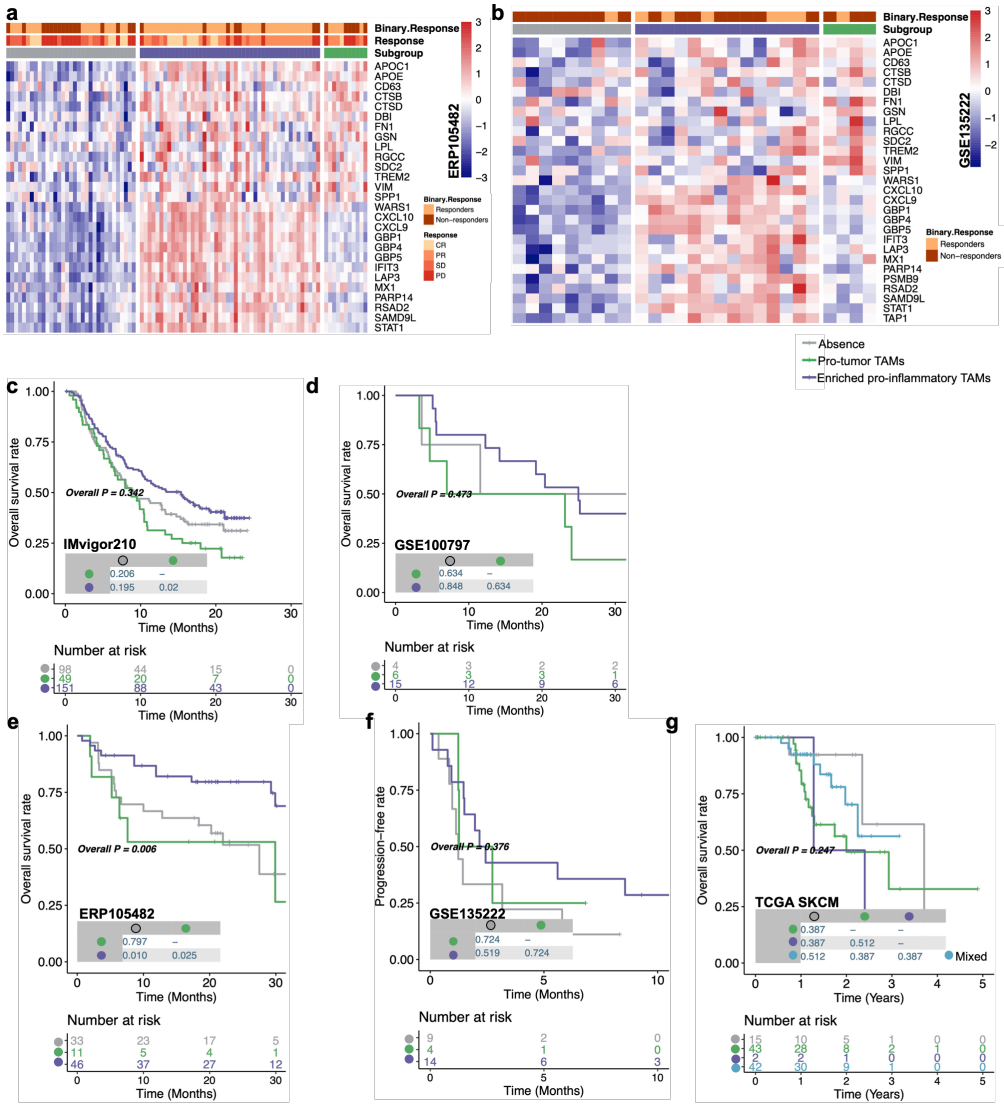

Supplementary Figure 13 Co-expressed genes and survival outcomes for TAMs subtypes across various cancer treatments and datasets. a Heatmap of pro-inflam and pro-tumor TAMs co-expressed genes for three different TAMs subtypes classification in the ERP105482 dataset. **b** Heatmap of pro-inflam and pro-tumor TAMs co-expressed genes for three different TAMs subtypes classification in the GSE135222 dataset. **c** Overall survival for patients in three different TAMs subtypes upon treatment with anti-PD1 in urothelial cancer patients. **d** Overall

survival for patients in three different TAMs subtypes upon treatment with adoptive T-cell therapy in melanoma patients. **e** Overall survival for patients in three different TAMs subtypes upon treatment with anti-PD1 and anti-PD1/anti-CTLA-4 combined therapy in melanoma patients. **f** Progression-free survival for patients in three different TAMs subtypes upon treatment with anti-PD-1/PD-L1 in lung cancer patients. **g** Overall survival for patients in four different TAMs subtypes among skin cutaneous melanoma (SKCM) patients.

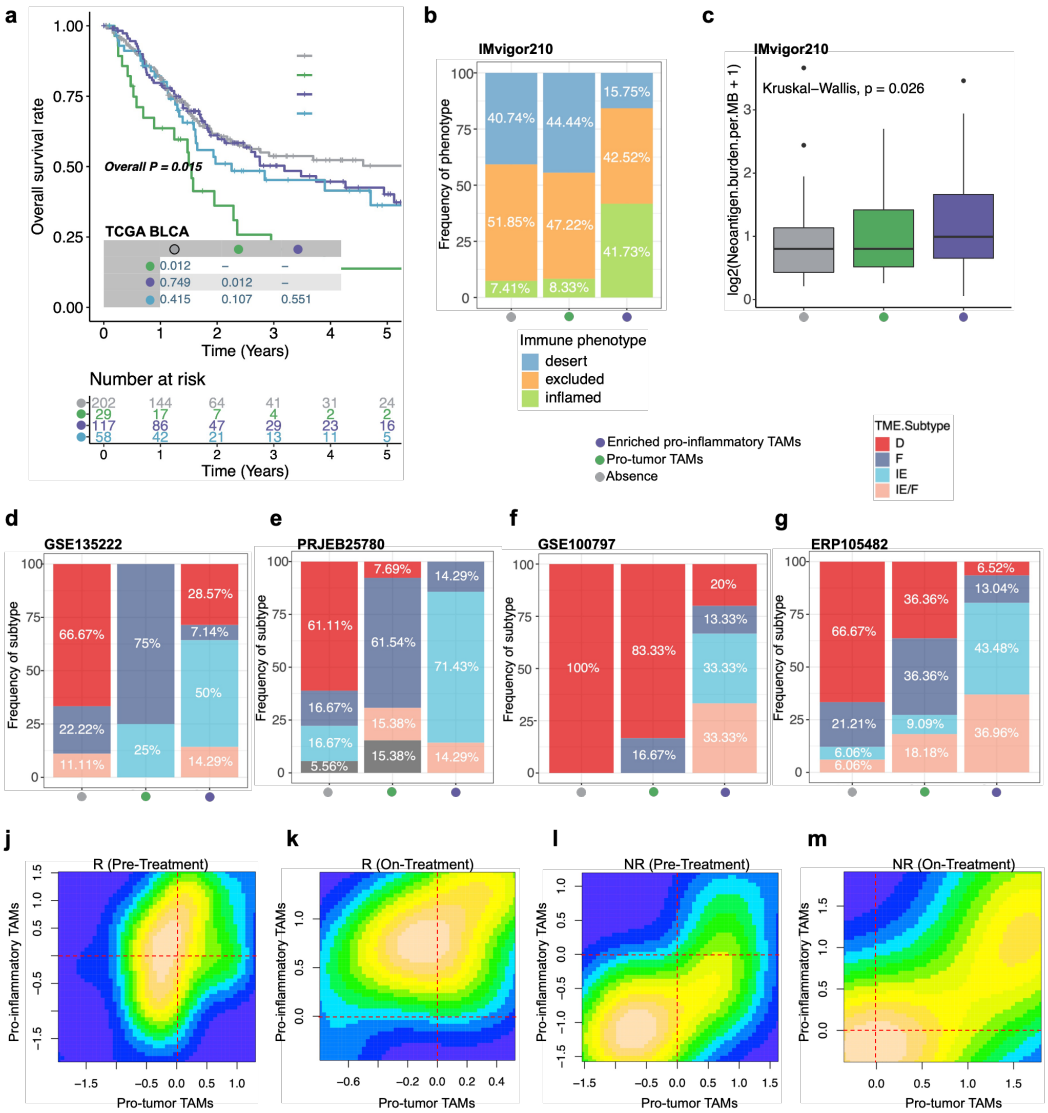

Supplementary Figure 14 Survival, immune phenotypes, neoantigen distribution, and TME subtype analysis across TAMs subtypes in various datasets. a Overall survival for patients in four different TAMs subtypes among muscle-invasive bladder cancer patients. **b** Rate of immune phenotype(desert/excluded/inflamed) to immunotherapy across three different TAMs subtypes in the IMvigor210 dataset. **c** Box plots showing the distribution of neoantigens per Mb across three different TAMs subtypes in the IMvigor210 dataset. Kruskal-Wallis test was performed to compare significance between subtypes. **d-g** Percentages of the four TME subtypes (D depleted; F fibrotic; IE: immune-enriched, non-fibrotic; IE/F immune-enriched, fibrotic) across the four TME subtypes in the GSE135222, PRJEB25780, GSE100797, and

ERP105482 datasets, respectively. **j-m** 2D density plot validating the relationship between pro-inflam and pro-tumor TAMs across response (pre-treatment and on-treatment) and non-response (pre-treatment and on-treatment) subgroups in the ERP105482 datasets.

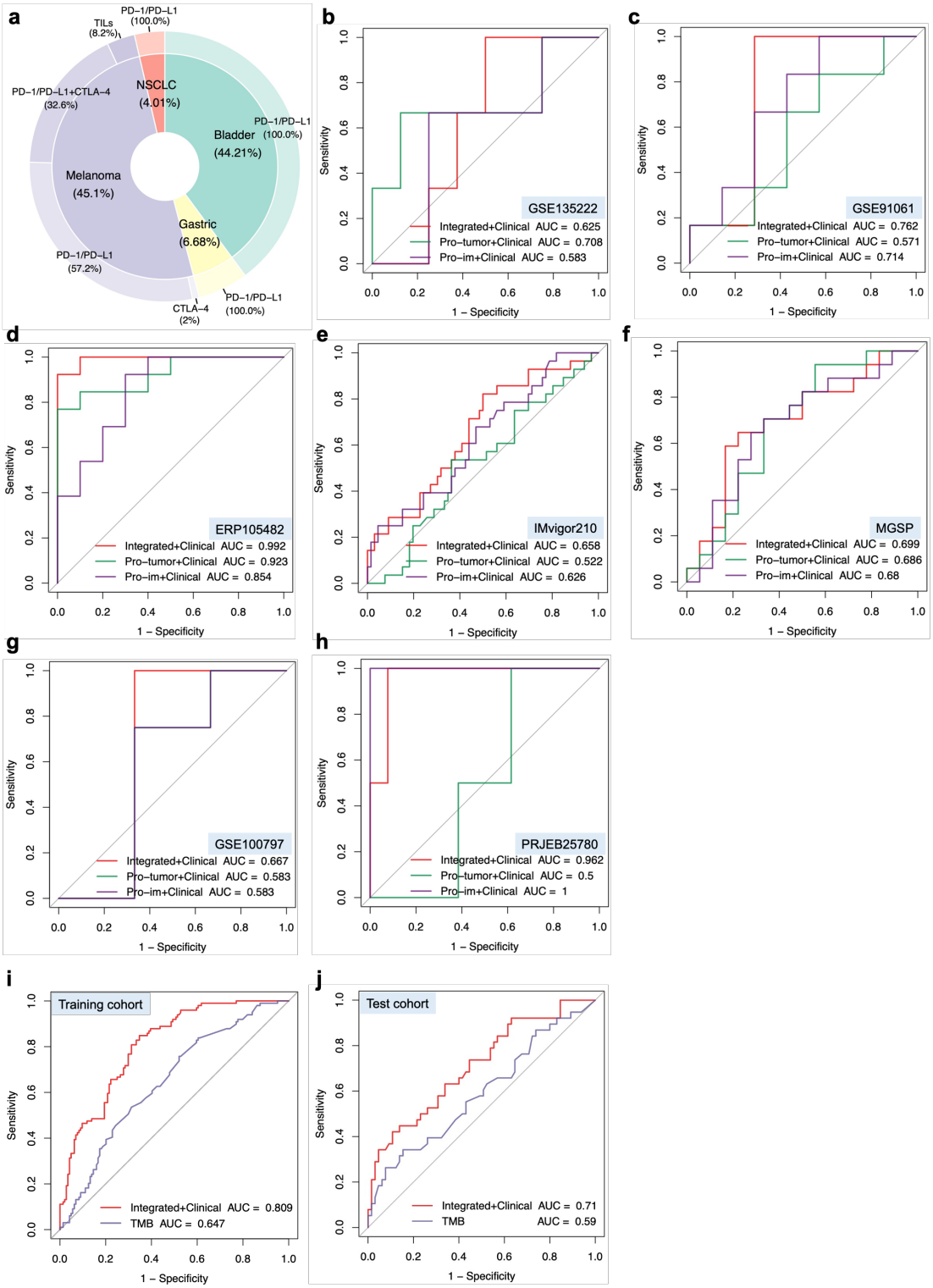

Supplementary Figure 15 Proportions of patients in ICB cohorts and ROC curves for predictive performance in ICB cohorts. a Pie charts demonstrating the proportions of patients from 8 ICB cohorts. **b-j** ROC curve of the sensitivity versus 1-specificity of the predictive performance of three feature types in 7 ICB cohorts.

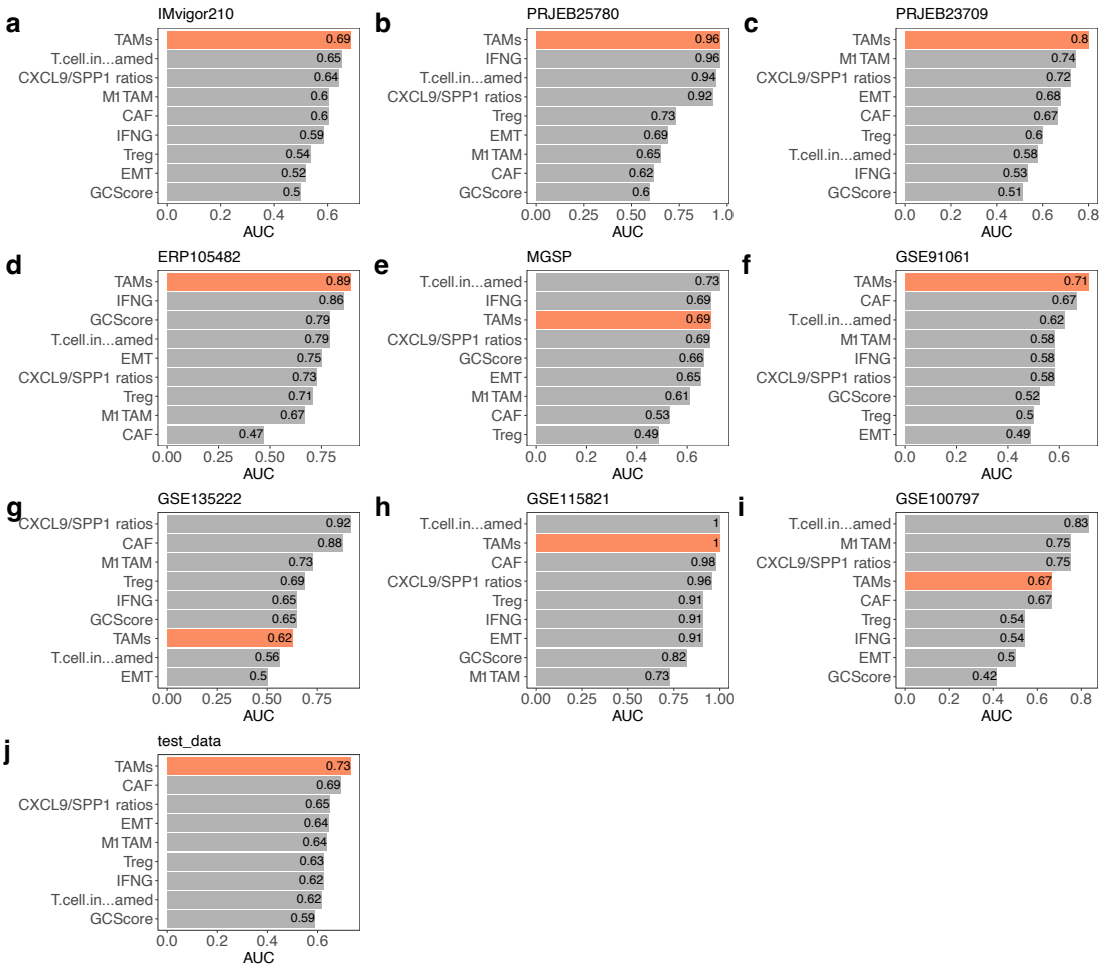

Supplementary Figure 16 Comparison of AUC for eight signatures predicting response to ICI therapy from published literature. a-j Comparison of the AUC of the with eight signatures in predicting response to ICI therapy from the published literature: IFN-γ, GCScore, EMT, and TME based markers (CXCL9:SPP1 ratio, Treg, T.cell.inflamed, cancer-associated fibroblast, M1 TAM).

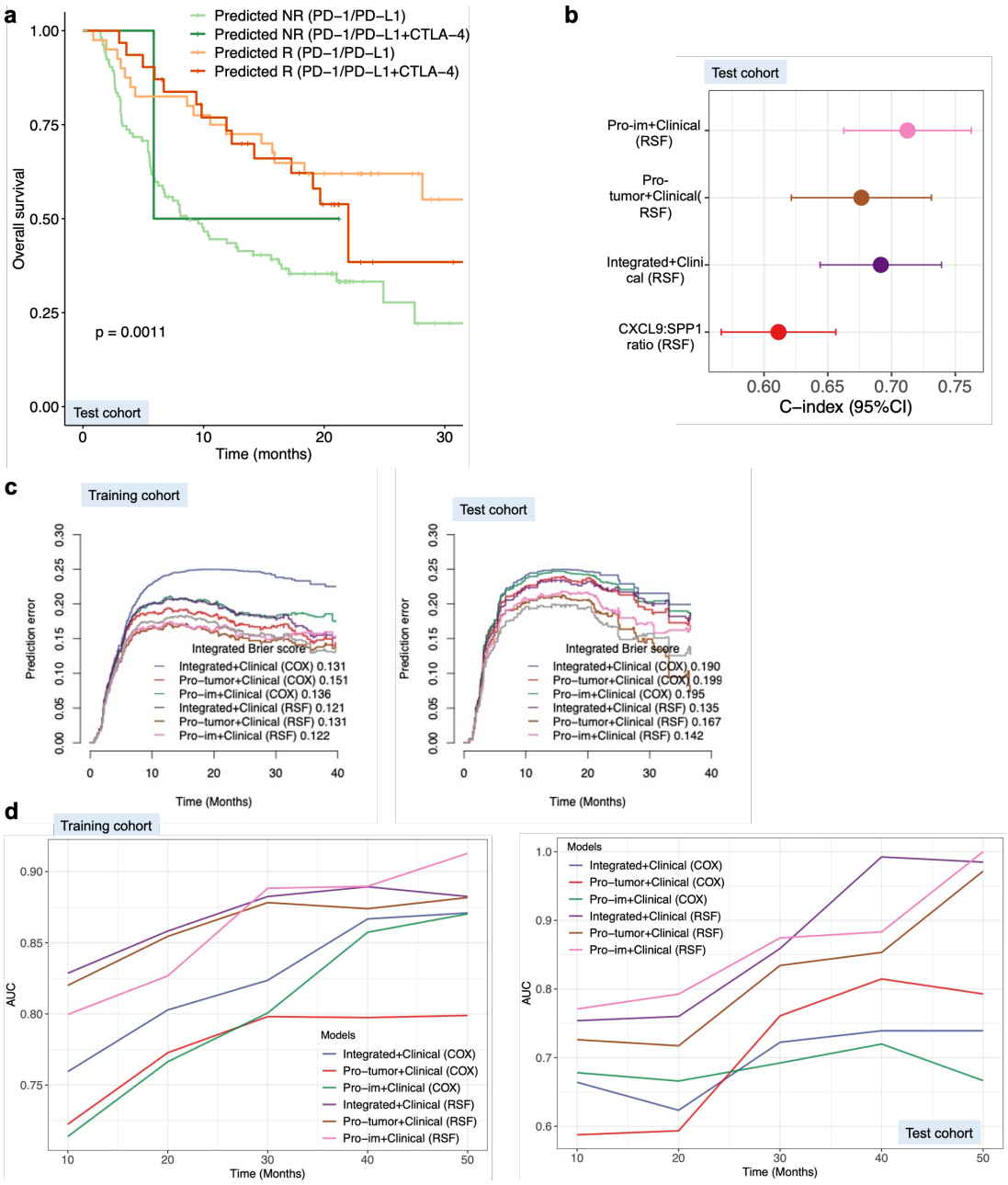

Supplementary Figure 17 OS stratification, model comparison, and predictive accuracy for different treatment regimens in the testing cohort. a OS stratified between responders and non-responders in patients in the testing cohort with different treatment regiments. **b** Comparison of c-index of multiple prediction models in the testing cohort. Each point represents the C-index of a different predictive model, with horizontal lines extending to show the confidence interval. **c** Brier score showing that the integrated TAMs RSF model for predicting OS has a smaller error compared to a reference model in the training and test cohorts. **d** Plots of monthly AUCs of COX and RSF models based on pro-inflam and pro-tumor TAMs signatures.

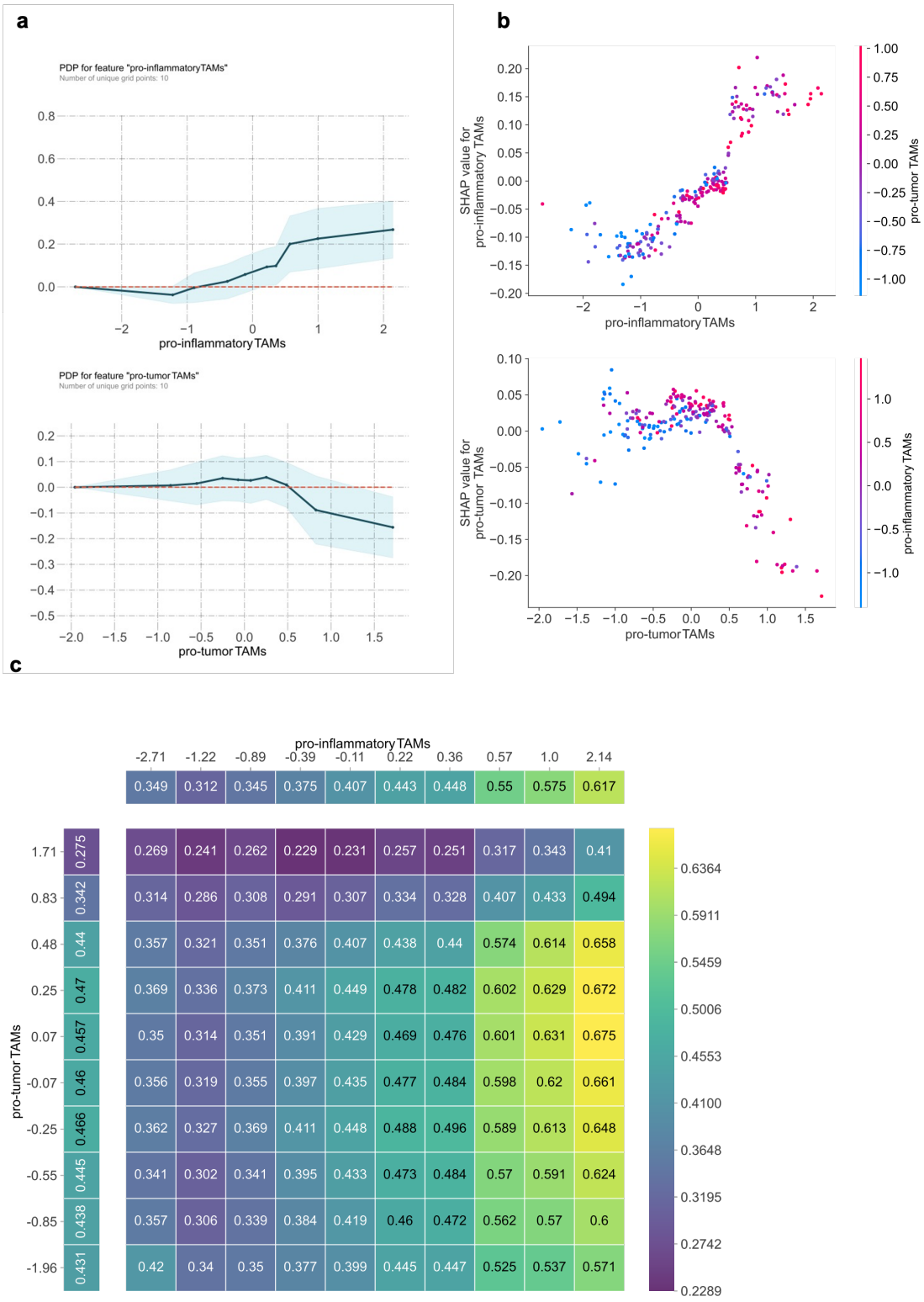

Supplementary Figure 18 Impact of pro-inflammatory and pro-tumor TAMs on response prediction and their interactions using PDPbox and SHAP. a Partial dependence plots of pro-inflam and pro-tumor TAMs that have an impact on response prediction using PDPbox. The blue areas in the plots indicate the extent of uncertainty. **b** The impact of interactions between pro-inflammatory and pro-tumor TAMs was estimated with SHAP. **c** Interaction between pro-inflam TAMs and pro-tumor TAMs using PDPbox.

Supplementary Table 1: Pro-inflam and pro-tumor TAMs-specific signatures	
Pro-inflam TAMs-specific signatures	pro-tumor TAMs-specific signatures
ATOX1	ANXA2
CXCL10	APOC1
CXCL9	APOE
GBP1	CD63
GBP4	CD9
GBP5	CSTB
IFIT3	CTSB
LAP3	CTSD
MX1	DBI
PARP14	ENO1
PSMB9	FN1
PSME2	GPNMB
RSAD2	GSN
SAMD9L	LGALS3
SERPING1	LPL
STAT1	MMP9
TAP1	PKM
TNFSF10	RGCC
TNFSF13B	SDC2
TYMP	SERF2
VAMP5	SH3BGRL3
WARS	TREM2
	VIM
	SPP1

Supplementary Table 2: All public datasets used in the paper			
scRNA-Seq			
Dataset names	cancer types	immunotherapies	Figures related to the dataset
PRJNA591860	lung cancer	None	Figure1A-E; Supplementary Figure1A-F; Supplementary Figure2A;
GSE146771	colorectal cancer	None	Figure1A-E; Supplementary Figure1A-F; Supplementary Figure2A
CNP0000650	hepatocellular carcinoma	None	Figure1A-E; Supplementary Figure1A-F; Supplementary Figure2A
GSE154763	esophageal	None	Figure1A-E; Supplementary

	carcinoma/thyroid carcinoma/renal cell carcinoma		Figure1A-F; Supplementary Figure2A
GSE154778	pancreatic ductal adenocarcinoma	None	Figure1A-E; Supplementary Figure1A-F; Supplementary Figure2A
GSE145370	esophageal carcinoma	None	Figure1A-E; Supplementary Figure1A-F; Supplementary Figure2A
GSE114725	breast cancer	None	Figure1A-E; Supplementary Figure1A-F; Supplementary Figure2A
PMID: 32060101	stomach adenocarcinoma	None	Figure1A-E; Supplementary Figure1A-F; Supplementary Figure2A; Supplementary Figure8G-H
GSE183904	stomach adenocarcinoma	None	Supplementary Figure2B
GSE203612	pancancer	None	Supplementary Figure2C
phs002065.v1.p1	renal cell carcinoma	anti-PD-1/anti-PD-1+TKI	Figure3A-E; Supplementary Figure8A-B
GSE120575	melanoma	anti-PD-1/anti-CTLA4+PD-1/anti-CTLA4	Figure3G-I; Supplementary Figure8C-F
bulk RNA-Seq			
Dataset names	cancer types	immunotherapies	Figures related to the dataset
PRJEB23709/ERP105482	melanoma	anti-PD-1 monotherapy/ anti-PD-1+anti-CTLA-4	Figure5G; Figure6A-H; Supplementary Figure13A; Supplementary Figure13E; Supplementary Figure14G-M; Supplementary Figure15A-J; Supplementary Figure16D; Supplementary Figure17-18
IMvigor210	urothelial cancer	anti-PD-L1	Figure5A-B; Figure6A-H; Supplementary Figure13C;

			Supplementary Figure14B-C; Supplementary Figure15A-J; Supplementary Figure16A; Supplementary Figure17-18
GSE100797	melanoma	adoptive T-cell therapy	Figure5E-F; Figure6A-H; Supplementary Figure13D; Supplementary Figure14F; Supplementary Figure15A-J; Supplementary Figure16I; Supplementary Figure17-18
GSE91061	melanoma	anti-PD-1	Figure6A-H; Supplementary Figure15A-J; Supplementary Figure16F; Supplementary Figure17-18
GSE135222	lung cancer	anti-PD-1	Figure5H; Figure6A-H; Supplementary Figure13B; Supplementary Figure13F; Supplementary Figure14D; Supplementary Figure15A-J; Supplementary Figure16G; Supplementary Figure17-18
PRJEB25780	gastric cancer	anti-PD-1	Figure5C-D; Figure6A-H; Supplementary Figure14E; Supplementary Figure15A-J; Supplementary Figure16B; Supplementary Figure17-18
MGSP	melanoma	anti-PD-1	Figure6A-H; Supplementary Figure15A-J; Supplementary Figure16E; Supplementary Figure17-18
GSE115821	melanoma	anti-PD-1/anti-CTLA-4	Figure6A-H; Supplementary Figure15A-J; Supplementary Figure16H; Supplementary Figure17-18
Spatial transcriptomics			
Dataset names	cancer types	immunotherapies	Figures related to the dataset
zenodo.4739739	breast cancer	None	Supplementary Figure9B
sciadv.abg3750	hepatocellular carcinoma	None	Supplementary Figure9C
EGAD00001008781	kidney cancer	None	Supplementary Figure10A